Contribution to the Improvement of Sensorless DTC-SVM for Three-Level NPC Inverter-fed Induction Motor Drive

DJAMILA CHERIFI , YAHIA MILOUD
Department of Electrical Engineering,
University of Dr.Tahar Moulay,
P. O. B. 138, 20000 Ennasr, Saida,
ALGERIA

Abstract: - This paper deals with the high performance of multi-level direct torque control (DTC) for induction machines without speed and stator flux sensors. The estimation is performed using a sliding mode observer, which is known for its robustness in high and low-speed operations, the control is based on a backstopping speed controller. This control technique was introduced years ago to circumvent the problems of sensitivity to parametric variations, it presents a high dynamic but their major problems are the variable switching frequency, the size and complexity of the switching tables, and undulations of the torque. The proposed approach is to replace switching tables with constant switching frequency control using three-level spatial vector modulation (SVM). Theoretical elements and simulation results are presented and discussed. As a result, the flux and torque ripple of three-level DTC-SVM control is greatly reduced compared to the flux and torque ripple of DTC-classic control. The advantages of the training system have been validated by the simulation results.

Key-Words: - squirrel cage motor, multi-level DTC, sliding mode observer (SMO), multi-level SVM, three-level NPC inverter, backstepping control.

Received: March 24, 2023. Revised: October 16, 2023. Accepted: November 11, 2023. Published: December 31, 2023.

1 Introduction

Currently, the induction motor is very popular because it has certain advantages over the DC motor in industrial applications, such as reliability and simple structure, this is what makes it used in all applications, [1], [2], [3]. This motor is used industrially due to its low cost, [4].

However, controlling this motor is very difficult given the performance required. This control problem comes down to the complicated and non-linear mathematical structure of the cage motor, and the dependence of these output parameters on those of the input ones, [5], different types of robust control have been developed to solve these problems. Rotor flux orientation vector control was developed to eliminate the internal coupling of the machine. However, although it gives a good performance of the induction machine, FOC has a certain number of drawbacks: poor robustness concerning variations in rotor parameters, dependence on an estimated angle, and the requirement for an expensive mechanical sensor. Direct torque control (DTC) comes to overcome the inherent drawbacks of vector control, [6], [7], [8].

DTC is among the best controls applied to asynchronous motors. Classic DTC is structured by hysteresis controllers, resulting in high ripples in torque and variable switching frequency, [9], [10]. This research work proposes a technique to improve the results of conventional DTC by introducing the three-level SVM to eliminate torque ripples and have fast dynamics compared to conventional DTC and also to achieve constant switching frequency and good motor performance.

PID regulators are not robust for controlling non-linear systems, they are sensitive to parametric variations. In this research work, we have addressed the control by backstepping controller for the robust regulation of the speed of the IM. it is a robust controller and insensitive to variations in system parameters, internal and external disturbances, and non-linearities.

The rotor speed of the IM must be measured by a speed sensor, which poses the problem of cost and maintenance. To overcome this problem the speed must be estimated using the motor currents and voltages. Several methods have been proposed for speed and position estimation of induction motors, [11], [12].

This research concerns direct multilevel torque control without speed and flux sensors. The strategy proposed in this work is based on the robust sliding mode observer and three-level space vector modulation.

2 Induction Motor Model

A dynamic model of the induction motor in the stator coordinates frame can be expressed by:

$$\frac{di_{s\alpha}}{dt} = -\lambda\, i_{s\alpha} - \omega_r\, i_{s\beta} + \frac{R_s}{\sigma L_s L_r}\phi_{s\alpha} + \frac{\omega_r}{\sigma L_r}\phi_{s\beta} + \frac{1}{\sigma L_s}u_{s\alpha}$$
$$\frac{di_{s\beta}}{dt} = -\lambda\, i_{s\beta} + \omega_r\, i_{s\alpha} + \frac{R_s}{\sigma L_s L_r}\phi_{s\beta} - \frac{\omega_r}{\sigma L_r}\phi_{s\alpha} + \frac{1}{\sigma L_s}u_{s\beta}$$
$$\frac{d\phi_{s\alpha}}{dt} = u_{s\alpha} - R_s i_{s\alpha}$$
$$\frac{d\phi_{s\beta}}{dt} = u_{s\beta} - R_s i_{s\beta} \qquad (1)$$

with $\lambda = \frac{R_s}{\sigma L_s} + \frac{R_r}{\sigma L_r}$

The torque equation is:

$$T_{em} = p\left(\phi_{s\alpha} i_{s\beta} - \phi_{s\beta} i_{s\alpha}\right) \qquad (2)$$

The mechanical relationship given by:

$$J\,\frac{d\Omega}{dt} = T_{em} - T_L - f\,\Omega \qquad (3)$$

Vector expression of the voltage delivered by the voltage inverter is:

$$\vec{V}_s = \sqrt{\frac{2}{3}}\mathrm{V_{dc}}\left[S_a + S_b e^{j\frac{2\pi}{3}} + S_c e^{j\frac{4\pi}{3}}\right] \qquad (4)$$

V_{dc} : represents the direct voltage.

DTC focuses on the adjustment of flux and torque by selecting voltage vectors and maintaining these two quantities in hysteresis bands to have high control precision, [13].

The flux estimate is:

$$\hat{\phi}_s = \sqrt{\hat{\phi}_{s\alpha}^{\,2} + \hat{\phi}_{s\beta}^{\,2}} \qquad (5)$$

The two estimated flux components are :

$$\begin{cases} \hat{\phi}_{s\alpha} = \int_0^t (v_{s\alpha} - R_s i_{s\alpha})dt \\ \hat{\phi}_{s\beta} = \int_0^t (v_{s\beta} - R_s i_{s\beta})dt \end{cases} \qquad (6)$$

With:

$$\theta_s = arctg\left(\frac{\hat{\phi}_{s\beta}}{\hat{\phi}_{s\alpha}}\right) \qquad (7)$$

The torque is estimated by:

$$T_{em} = p\left(\hat{\phi}_{s\alpha} i_{s\beta} - \hat{\phi}_{s\beta} i_{s\alpha}\right) \qquad (8)$$

Compared with two-level DTC, three-level DTC motor drives have a special aspect, that relates to improving electromagnetic performance, including reducing torque ripple and improving low-speed performance, in a similar manner to that of two-level DTC, [14], [15].

3 The Composition of a Multilevel Inverter with NPC Structure (3 levels)

The three phases of the multilevel structure of the NPC inverter are shown in Figure 1. This structure is composed of two identical capacitors with a common midpoint denoted “M”. The inverter has three arms A, B, and C. Each consists of four fully controllable switches with four anti-parallel diodes to ensure the reversibility of currents in the load, and two clamp diodes to develop the multilevel voltage, which are connected to the midpoint of the DC bus, [16], [17], [18].

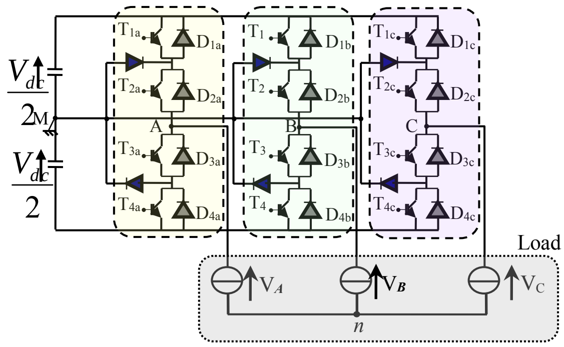

Fig. 1: Structure of a three-phase inverter with NPC structure -3 level-

Controlling the switches (considered perfect) of an arm, three different voltage levels can be imposed on the phase, as shown in Figure 2:

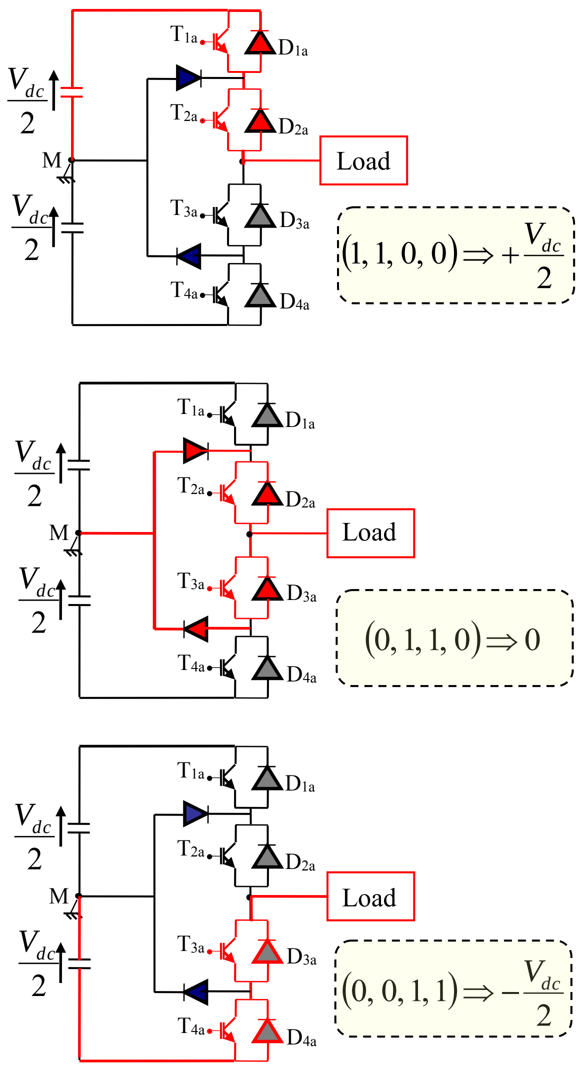

Fig. 2: Switching and passage of energy in phase "A" switches.

3.1 SVM Multilevel of NPC inverter

Modeling of the 3 level voltage inverter showed that for the different drive combinations, the inverter can generate only 27 voltage vectors in the plane (α, β), (3^3=27), three of which are zero (Figure 3). It is therefore necessary to apply feasible voltage vectors for adequate durations over this interval T_s, [19], [20].

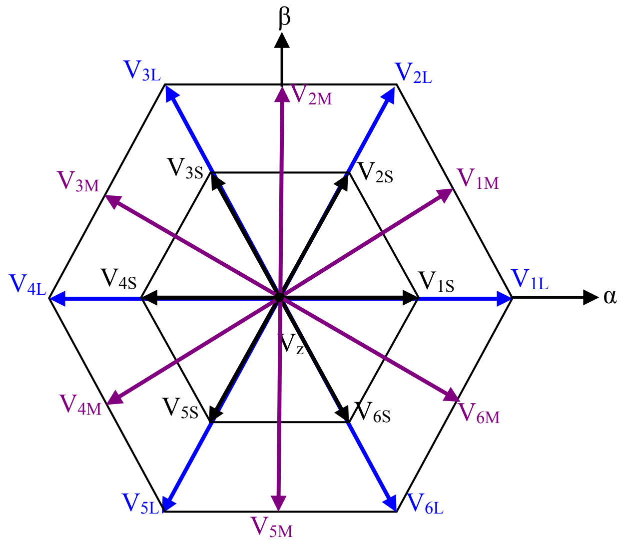

Fig. 3: Diagram of the placement of the different voltage vectors

The different vectors form an exagon of six triangles (A to F), and each triangle is also composed of four other triangles, thus giving in the totality of the vector diagram to 24 regions, [21], [22], as shown in Figure 4.

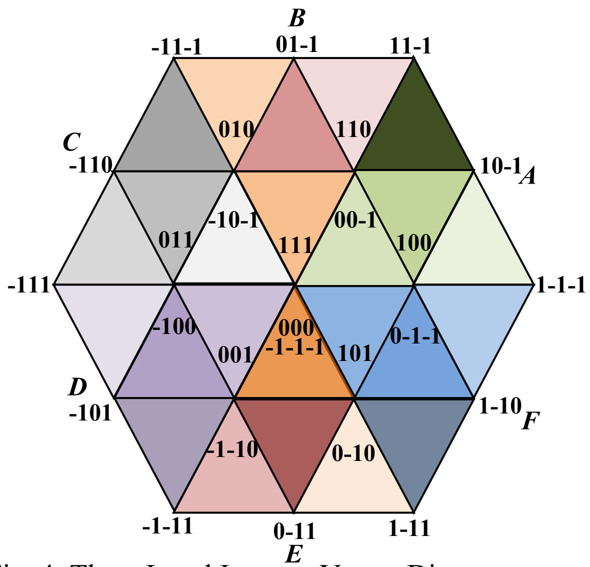

Fig. 4: Three Level Inverter Vector Diagram

The vector PWM technique applied to multi-level inverters follows the following calculation steps:

1- Determination of the duty cycles T_a, T_b, and T_c for each region.

2- Determination of the switching period of each switch.

3.2 Calculation of T_a, T_b, and T_c for each Region

The calculation is done in the region (A). The projection of the reference vector (V_{ref}) onto the first region of the sector (A) is shown in Figure 5, [21], [22].

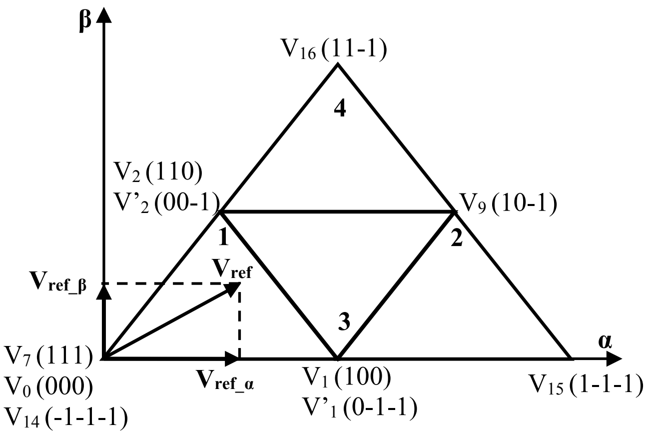

Fig. 5: Projection of the reference vector into the first region of sector A

According to the figure, the vectors concerned are V_0 ou V_7 ou V_{14}, V_1, and V_2, [21], [22].

$$\int_0^{T_m} V_{ref}.dt = \int_0^{T_a} V_1.dt + \int_{T_a}^{T_a+T_c} V_2.dt + \int_{T_a+T_c}^{T_m} V_0.dt \tag{9}$$

$$T_m.\overline{V_{ref}} = T_a.\overline{V_1} + T_c.\overline{V_2} \tag{10}$$

$$T_m.\left|\overline{V_{ref}}\right|.\begin{bmatrix}\cos(\theta)\\ \sin(\theta)\end{bmatrix} = T_a.\frac{1}{\sqrt{6}}.E.\begin{bmatrix}1\\0\end{bmatrix} + T_c.\frac{1}{\sqrt{6}}.E.\begin{vmatrix}\cos\left(\frac{\pi}{3}\right)\\ \sin\left(\frac{\pi}{3}\right)\end{vmatrix} \tag{11}$$

$$T_m.V_{ref}.\cos(\theta) = \frac{E}{\sqrt{6}}.T_a + \frac{E}{\sqrt{6}}.T_c.\frac{1}{2} \tag{12}$$

$$T_m.V_{ref}.\sin(\theta) = \frac{E}{\sqrt{6}}.T_c.\frac{\sqrt{3}}{2} \tag{13}$$

$$T_m = T_a + T_b + T_c \tag{14}$$

$$\Rightarrow \frac{E}{2\sqrt{2}}.T_a = T_m.V_{ref}.\sin(\theta).\frac{\sqrt{3}}{2}$$

$$\Rightarrow T_c = \frac{2\sqrt{2}.T_m.V_{ref}}{E}.\sin(\theta) \tag{15}$$

We replace the expression of (T_c) in (12) we find:

$$T_m.V_{ref}.\cos(\theta) = \frac{E}{\sqrt{6}}.T_a + \frac{E}{\sqrt{6}}.\frac{2\sqrt{2}.T_m.V_{ref}}{E}\sin(\theta).\frac{1}{2}$$

$$\Rightarrow T_a = \frac{2\sqrt{2}.T_m.V_{ref}}{E}\sin\left(\frac{\pi}{3}-\theta\right) \tag{16}$$

$$\Rightarrow T_b = T_m - T_a - T_c = T_m\left[1 - \frac{2\sqrt{2}.V_{ref}}{E}\sin\left(\frac{\pi}{3}+\theta\right)\right] \tag{17}$$

We take: $K = \dfrac{2\sqrt{2}.V_{ref}}{E}$

So: $T_a = K.T_m \sin\left(\dfrac{\pi}{3}-\theta\right)$,

$T_b = T_m\left[1 - K.\sin\left(\dfrac{\pi}{3}+\theta\right)\right]$, $T_c = K.T_m \sin(\theta)$

Similarly, the switching times for the other regions of sector A are found. The switching times for the rest of the sectors (from B to F) are calculated in the same way.

3.3 Calculation of Switching Times for each Switch

Figure 6 shows the waveforms showing the order of switching states for Region 1 in the sector (A).

With: (S_{i1}, S_{i2}): are respectively the switching times of the switches at the top (K_{i1}, K_{i2}) for arm i. With: (i=a, b, c)

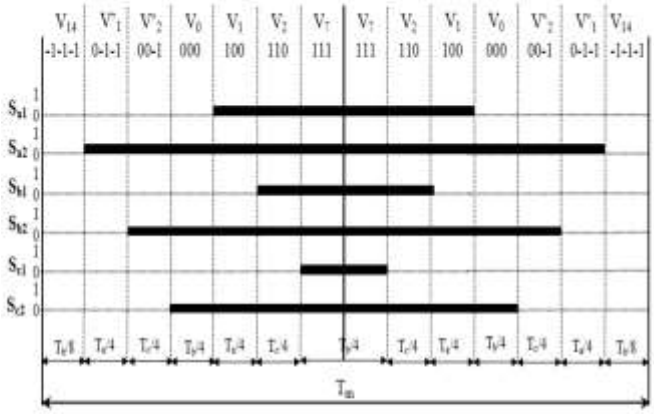

Fig. 6: Switching times for the switches at the top of inverter in region 1 of utility (A).

The previous figure helps us calculate the switching time

$$S_{a1} = 2.\left(\frac{T_a}{4}+\frac{T_c}{4}+\frac{T_b}{8}\right) \Rightarrow S_{a1} = \frac{T_a}{2}+\frac{T_c}{2}+\frac{T_b}{4} \tag{18}$$

$$S_{a2} = 2.\left(\frac{T_a}{4}+\frac{T_c}{4}+\frac{T_b}{4}+\frac{T_a}{4}+\frac{T_c}{4}+\frac{T_b}{8}\right) \tag{19}$$

$$\Rightarrow S_{a2} = S_{a1} + \frac{1}{2}\left(T_a + T_c + T_b\right) \quad (20)$$

$$S_{b1} = 2.\left(\frac{T_c}{4} + \frac{T_b}{8}\right) \Rightarrow S_{b1} = \frac{T_c}{2} + \frac{T_b}{4} \quad (21)$$

$$S_{b2} = 2.\left(\frac{T_c}{4} + \frac{T_b}{4} + \frac{T_a}{4} + \frac{T_c}{4} + \frac{T_b}{8}\right)$$

$$\Rightarrow S_{b2} = S_{b1} + \frac{1}{2}\left(T_a + T_c + T_b\right) \quad (22)$$

$$S_{c1} = \frac{T_b}{4} \quad (23)$$

$$S_{c2} = 2.\left(\frac{T_b}{4} + \frac{T_a}{4} + \frac{T_c}{4} + \frac{T_b}{8}\right)$$

$$\Rightarrow S_{c2} = S_{c1} + \frac{1}{2}\left(T_a + T_c + T_b\right) \quad (24)$$

Similarly, the switching times of the switches are calculated for the other cases.

The advantage of multilevel DTC without a speed sensor is that it will give good results compared to two-level SVM and conventional DTC

4 Sliding mode observer (SMO)

The mathematical model of the IM is the basis for constructing the observer. It uses imposed inputs and measured outputs whose correction terms are discontinuous function sign for torque and speed estimation.

The state vectors are: " ϕ_s " and " i_s "

SMO based on this equation, [23], [24] :

$$\begin{cases} \frac{d}{dt}\underline{\phi}_s = -R_s \underline{i}_s - j\omega_r \underline{\phi}_s + \underline{u}_s \\ \frac{d}{dt}\underline{i}_s = -\left(\frac{1}{T_s\sigma} + \frac{1}{T_r\sigma}\right)\underline{i}_s + \frac{1}{L_s\sigma}\left(\frac{1}{T_r} - j\omega_r\right)\underline{\phi}_s + \frac{1}{L_s\sigma}\underline{u}_s \end{cases} \quad (25)$$

where: $T_s = \frac{L_s}{R_s}$, $T_r = \frac{L_r}{R_r}$

note the existence of the back-EMF $j\omega_r \underline{\phi}_s$ in (25). So we move on to the next model

$$\begin{cases} \frac{d}{dt}\hat{\underline{\phi}}_s = -R_s \underline{i}_s - j\omega_r \underline{\phi}_s + \underline{u}_s - K\,\mathrm{sgn}(S) \\ \frac{d}{dt}\hat{\underline{i}}_s = -\left(\frac{1}{T_s\sigma} + \frac{1}{T_r\sigma}\right)\hat{\underline{i}}_s + \frac{1}{L_s\sigma}\left(\frac{1}{T_r} - j\omega_r\right)\hat{\underline{\phi}}_s + \frac{1}{L_s\sigma}\underline{u}_s - \frac{1}{L_s\sigma}K\,\mathrm{sgn}(S) \end{cases} \quad (26)$$

The corrector obtained is

$$S = \left(K_p + \frac{K_i}{s}\right)\left(\hat{i}_s - i_s\right) \quad (27)$$

4.1 Gain Selection

Based on the Lyapunov function, we give the gain of the observer which ensures the stability:

$$K > \max\left(\left|\frac{e_{\phi_{s\alpha}}}{T_r} - \omega_r \phi_{s\beta}\right| \left|\frac{e_{\phi_{s\beta}}}{T_r} - \omega_r \phi_{s\alpha}\right|\right) \quad (28)$$

flux error is expressed by $e_{\phi_{s\alpha}}$

4.2 Rotor Speed Estimation of IM

ω_r calculated by (29), this is among the advantages of this type of observer :

$$\hat{\omega}_r = \hat{\omega}_s - \hat{\omega}_{g1} = \frac{1}{\phi_r^2}\left(\frac{d\hat{\phi}_{r\beta}}{dt}\hat{\phi}_{r\alpha} - \frac{d\hat{\phi}_{r\alpha}}{dt}\hat{\phi}_{r\beta}\right) - \frac{R_s \hat{T}_{em}}{p.\phi_r^2} \quad (29)$$

based on ϕ_s and i_s, ϕ_r estimated, as is well demonstrated by this equation:

$$\hat{\phi}_r = \frac{L_r\hat{\phi}_s - L_s.L_r.\sigma.i_s}{M} \quad (30)$$

5 Speed Controller based on Backstepping

In this part, the Backstepping controller is used to control the induction motor speed for sensorless control.

Lyapunov's theory allows us to build a robust controller, [25], [26], [27] :

$$\frac{d\Omega(t)}{dt} = \frac{1}{J}\left[T_{em}(t) + T_L(t) + f\,\Omega(t)\right] \quad (31)$$

where:

$$\frac{d\Omega(t)}{dt} = \dot{\Omega}(t) = aT_{em}(t) + bT_L(t) + c\Omega(t) \quad (32)$$

The parameters of the motor are expressed by a, b, and c:

$$a = \frac{1}{J}, b = -\frac{1}{J}, c = \frac{f}{J}$$

We derive the speed error by this equation:

$$e(t) = \Omega_{ref}(t) - \Omega(t) \quad (33)$$

We calculate the derivative of the speed error by:

$$\dot{e}(t) = \dot{\Omega}_{ref}(t) - \dot{\Omega}(t) \quad (34)$$

We can write:

$$\dot{e} = \dot{\Omega}_{ref}(t) - aT_{em}(t) - bT_L(t) - c\Omega(t) \quad (35)$$

The Lyapunov function is :

$$V(t) = \frac{1}{2}e^2(t) \quad (36)$$

We derive the Lyapunov function and we find:

$$\dot{V}(t) = e(t)\dot{e}(t) = e(t)\left[\dot{\Omega}_{ref}(t) - aT_{em}(t) - bT_L(t) - c\Omega(t)\right] \quad (37)$$

The derivative of the Lyapunov function V is negative. This is expressed by the definition of a constant "K" in equation (36)

$$\dot{V}(t) = -K.e^2(t) \le 0 \quad (38)$$

The general formula for reference torque T^*_{em} is expressed by:

$$T^*_{em}(t) = \frac{1}{a}\left[\dot{\Omega}_{ref}(t) - b.T_L(t) - c.\Omega(t) + K.e(t)\right] \quad (39)$$

6 Simulation Results and Discussion

The Global structure of multilevel DTC-SVM without speed sensor and stator flux based on the robust sliding mode observer and with motor torque estimation is shown in Figure 7.

The three-phase squirrel cage motor of 1.5 kW, parameters are indicated in Table 1.

Table 1. IM motor parameters

Item	Symbol	Data
IM Mechanical Power	P_W	1.5 Kw
Nominal speed	ω	1420 rpm
Nominal Frequency	f	50 Hz
Pole pairs number	P	2
Stator resistance	R_s	4.85Ω
Rotor resistance	R_r	3.805Ω
Stator self-inductance	L_s	274 mH
Rotor self-inductance	L_r	274 mH
Mutual inductance	L_m	258 mH
Moment of inertia	J	0.031 kg.m^2
Friction coefficient	F	0.00114kg.m^2/s

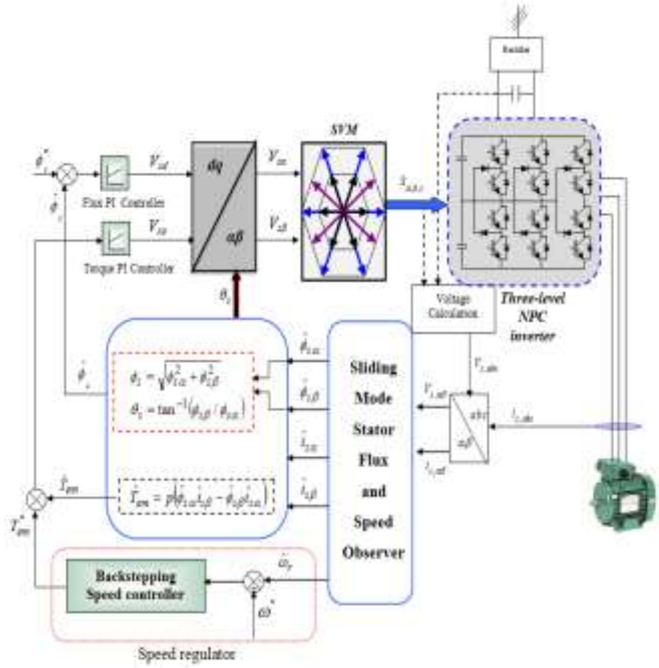

Fig. 7: Global scheme of sensorless DTC of induction motor with multilevel SVM based on rotor speed and stator flux observers

6.1 Performance of DTC with Three-Level SVM Sensorless Induction Motor based on SM Observer

Figure 8 gives the good behavior of IM when estimating the speed by the SMO with high dynamics, also there is negligible sensitivity to load disturbances.

The electromagnetic torque response was very fast. The load torque has no influence on the stator flux in the plane (α, β), which proves that the decoupling between torque and flux has been well achieved.

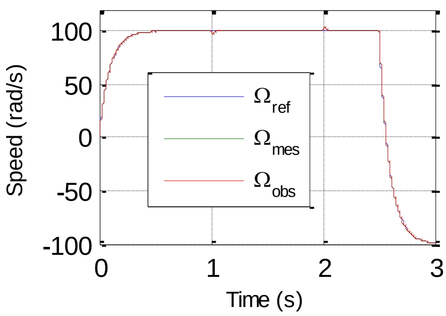

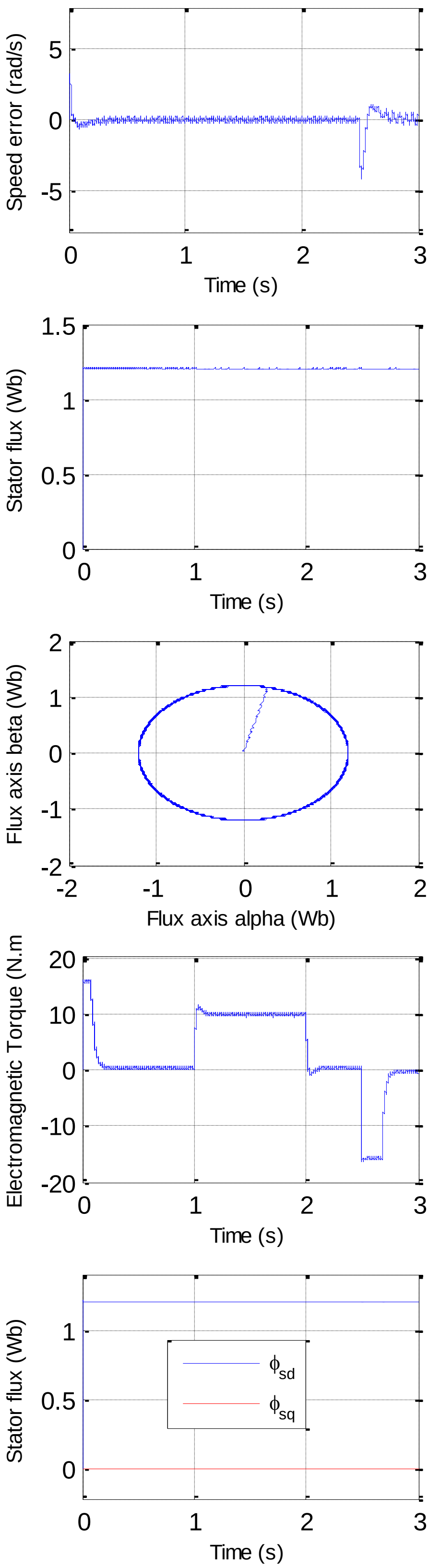

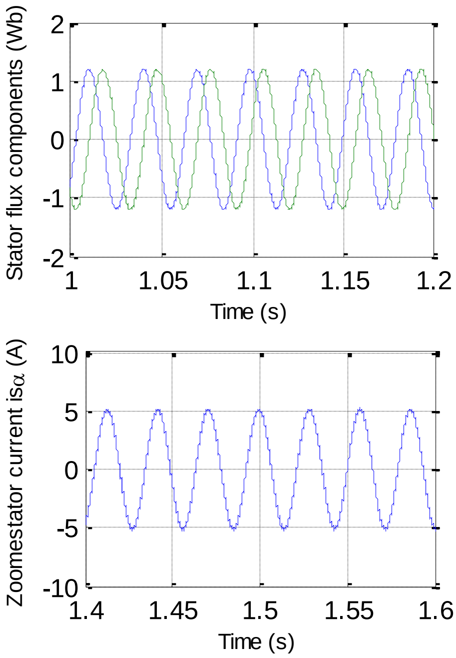

Fig. 8: Different simulation results of the proposed structure drives: rotor speed, speed error, stator flux, torque, flux, flux circular trajectory

6.2 Robustness Tests

a. Trapezoidal speed profile

This test concerns the profile of the reversal of the direction of rotation from -100 rad/s to 100 rad/s, as shown in Figure 9 it gives a good control results.

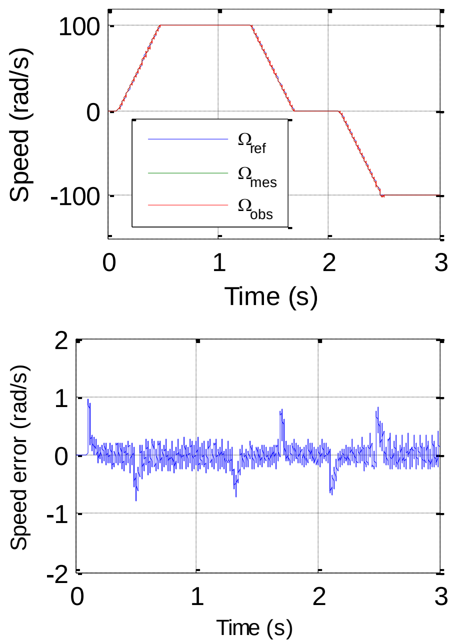

Fig. 9: Approach proposed with variable speed and rotation reversal

b. Low-speed test

In this simulation, the small speed value chosen to drive the motor is 10 rad/s, is shown in Figure 10.

The results prove that the approach studied is very effective in all speed regions and the estimation was well done for 10 rad/s and gives a static error equal to zero, with rapid rejection of load disturbance.

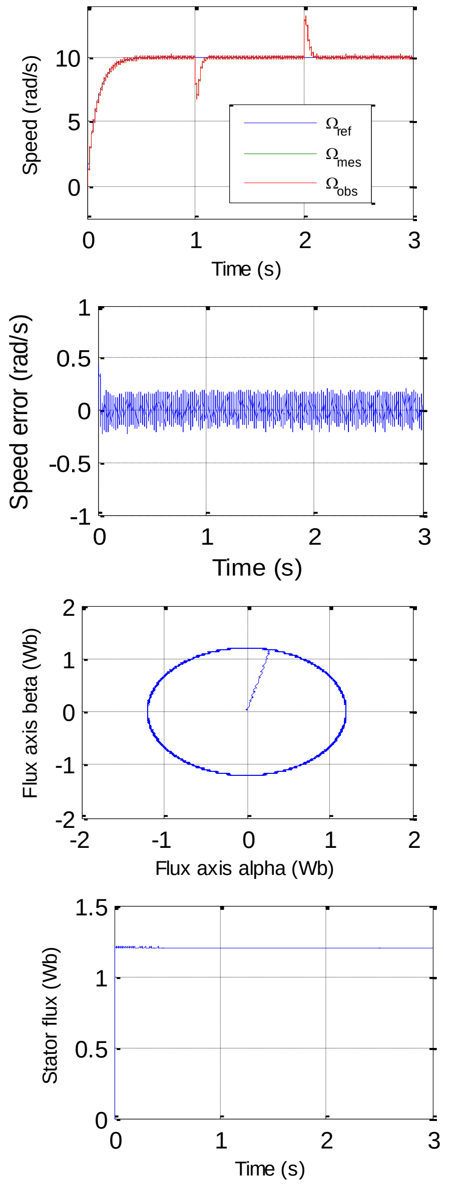

Fig. 10: Results of low-speed test

c. Resistive parameter change

We amplified Rs by half of its nominal value, and the result as found was shown in Figure 11 which demonstrates that the change in this parameter does not influence the performance of the training, the observer at a good estimation of the speed and the speed regulation loop by Backstepping clearly shows its robustness.

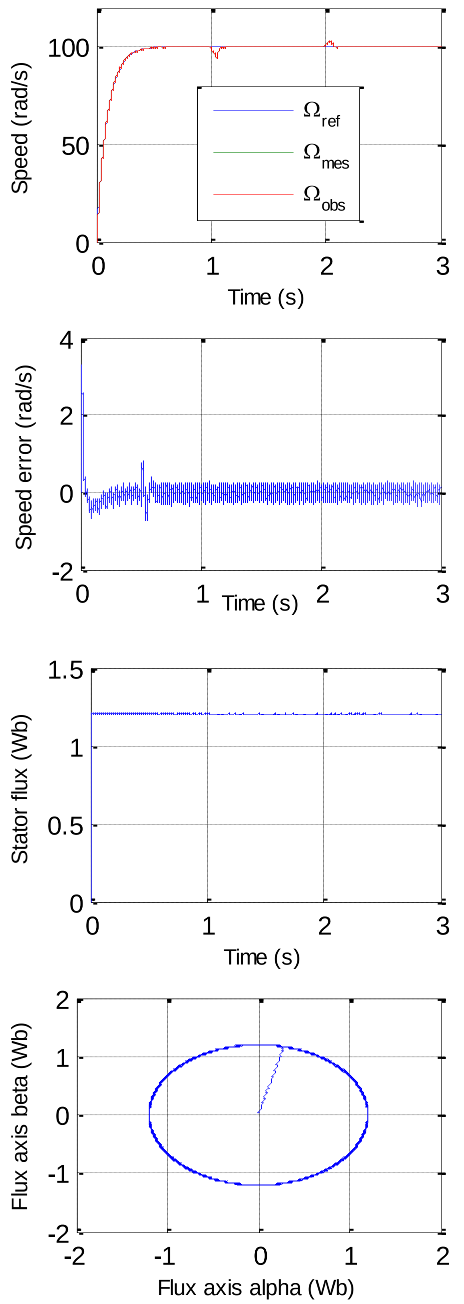

Fig. 11: Study of the influence of the increase in Rs on the proposed sensorless control drives

7 Conclusion

The research presented in this paper addresses the DTC with multilevel SVM command of asynchronous motor for sensorless control of speed and flux, the used observation based on sliding mode, using an algorithm robust adjustment system based on the backstepping controller for the servo-control and speed regulation of the machine.

The essential aim of this research work is to improve the performance of a drive system based on an induction motor controlled by DTC using multilevel inverters and the digital and robust control approach by SVM.

1. Eliminated the disadvantage of variable switching due to hysteresis comparators which causes high ripples

2. Replacement of classical control laws by non-linear ones to ensure the stability and robustness of the system,

3. Eliminated the high number of sensors by inserting a sensorless algorithm

This allows us to say that the study control system provides effective improvements to the DTC control of the IM, we then see:

1. elimination of flux and torque ripples
2. good speed regulation in all chosen ranges
3. robustness to parameter variations and load disturbances.
4. decoupling between flux and torque of the motor.
5. Sliding mode observer shows good accuracy and excellent estimation of speed and flux

For the continuation of research relating to this work, we propose as perspectives:

• Application of other complete order observers.

• Development of control strategies for dual-supply induction motors

References:

[1] Gdaim, S., Mtibaa, A., Mimouni, M.F. (2015). Design and experimental implementation of DTC of an induction machine based on fuzzy logic control on FPGA. *IEEE Trans. Fuzzy Syst.*, 23, (3), pp. 644–655.

[2] Zaki Diab, A. A., El-Sayed, A. M., Abbas, H., Abd El Sattar, M. (2019). Robust Speed Controller Design Using H_infinity Theory for High-Performance Sensorless Induction Motor Drives. *Energies*, pp. 1-21.

[3] Moaveni, B., Khorshidi, M. (2015). Robust speed controller design for induction motors based on IFOC and Kharitonov theorem. *Turkish Journal of Electrical Engineering & Computer Sciences*, pp. 1173-1186.

[4] Yetgin, A. G., Turan, M., Cevher, B., Çanakoğlu, A. İ., Gün, A. (2019). Squirrel Cage Induction Motor Design and the Effect of Specific Magnetic and Electrical Loading Coefficient. *International Journal of Applied Mathematics Electronics and Computers IJAMEC*, vol 7, no 1, pp. 1–8.

[5] Omari, A., Khalil, B. I., Hazzab, A., Bouchiba, B., Benmohamed, F.E. (2018). Real-time implementation of MRAS rotor time constant estimation for induction motor vector control based on a new adaptation signal. *The International Journal for Computation and Mathematics in Electrical and Electronic Engineering*, Volume 38 Issue 1, pp. 287-303. https://doi.org/10.1108/COMPEL-03-2018-0133.

[6] Said, M., Aziz, D., El Ouanjli, N., A Mossa, M., Sagar Bhaskar, M., Ngo, K. L., Nguyen, V. Q. (2022). A New Robust Direct Torque Control Based on a Genetic Algorithm for a Doubly-Fed Induction Motor: Experimental Validation. *Energies*, 15, 5384.

[7] Takahashi, I., Noguchi, T. (1986). A new quick response and high efficiency control strategy of an induction motor. *IEEE Trans. Ind. Applicat*, vol. IA-22, pp. 820–827.

[8] Depenbrok, M. (1988). Direct self-control (DSC) of inverter fed induction machine. *IEEE Trans. Power Electron.,* vol. PE-3, pp. 420–429.

[9] Krim, S., Gdaim, S., Mtibaa, A., Mimoun, M. F. (2016). FPGA-Based DTC-SVM: A Comparative study between two approaches, 2016 4th International Conference on Control Engineering & Information Technology (CEIT), 16-18 December 2016, Tunisia, https://doi.org/10.1109/CEIT.2016.7929060.

[10] Hongxia, Y., Zhicheng, C. (2015). Three-Phase Induction Motor DTC-SVPWM Scheme with Self-tuning PI-Type Fuzzy Controller. *International Journal of Computer and Communication Engineering*, Vol. 4, No.3.

[11] Cherifi, Dj., Miloud, Y. (2018). Speed sensorless control of a doubly fed induction motor drives using MRAS estimator. *International Journal of Electrical Components and Energy Conversion*, Vol. 4, No. 1, pp. 1-12.

[12] Kuchar, M.; Palacky, P.; Simonik, P.; Strossa, J. Self-Tuning. (2021). Observer for Sensor Fault-Tolerant Control of Induction Motor Drive. *Energies*, 14, 2564.

[13] Zemmit, A., Messalti, S., Harrag, A. (2018). A new improved DTC of doubly fed induction machine using GA-based PI controller. *Ain Shams Engineering Journal*, Vol. 9, No. 1, pp. 1877–1885.

[14] Rashag, H. F., Tan, N. M. L., Koh, S. P., Abdalla, A. N., Chong, K. H., K Tiong, S. (2014). DTC-SVM Based on PI Torque and PI Flux Controllers to Achieve High Performance of Induction Motor. *Research*

Journal of Applied Sciences, Engineering and Technology, Vol. 7, No. 4, pp. 875-891.

[15] Mohan, D., Zhang, X., & Foo, G. H. B. (2016). A simple duty cycle control strategy to reduce torque ripples and improve low-speed performance of a three-level inverter fed DTC IPMSM drive. *IEEE Transactions on Industrial Electronics*, 64(4), 2709–2721.

[16] Zhang, M., Cui, Y., Wang, Q., Tao, J., Wang, X., Zhao, H., Li, G. (2019). A Study on Neutral-Point Potential in Three-Level NPC Converters. *Energies*, 12, 3367.

[17] Pabbewar, A. S., Kowsalya, Dr. M. (2016). Three Level Neutral Point Clamped Inverter using Space Vector Modulation with Proportional Resonant Controller. ScienceDirect, *Energy Procedia* (103) pp. 286-291.

[18] Górecki, K., Rogowski, K., Beniak, R. (2019). Three-level NPC Inverter SVM Implementation on Delfino DSC. *ScienceDirect*, IFAC PapersOnLine 52-27, pp. 252–256.

[19] Ouerdani, I,. Ben Abdelghani, Hafedh., Ben Abdelghani, A. B., Montesinos-Miracle, D Slama-Belkhodja, I. (2016). Space Vector Modulation Technique for 3-Level NPC Converter with Constant Switching Frequency. Hindawi Publishing Corporation. *Advances in Power Electronics*, Vol. 2016, Article ID 6478751, 13 pages.

[20] Ouerdani, I., Ben Abdelghani, H., Ben Abdelghani, A. B., Montesinos-Miracle, D., Belkhodja, I. S. (2016). Space Vector Modulation Technique for 3-Level NPC Converter with Constant Switching Frequency. Hindawi Publishing Corporation, *Advances in Power Electronics*, Vol. 2016, https://doi.org/10.1155/2016/6478751.

[21] Kadum, A. A. (2020). PWM control techniques for three phase three level inverter drives. *TELKOMNIKA Telecommunication, Computing, Electronics and Control*, Vol. 18, No. 1, pp. 519-529.

[22] Rongwu Zhu., Xiaojie Wu., Yi Tang. (2015). Duty cycle-based three-level space-vector pulse-width modulation with overmodulation and neutral-point balancing capabilities for three-phase neutral-point clamped inverters. *IET Power Electron.*, Vol. 8, Iss. 10, pp. 1931–1940

[23] El Daoudi, S., Lazrak, L., Ait Lafkih, M. (2020). Sliding mode approach applied to sensorless direct torque control of cage asynchronous motor via multi-level inverter. *Protection and Control of Modern Power Systems,* vol. 5, Article number: 13

[24] Ammar, A., Bourek, A., Benakcha, A. (2019). Robust load angle direct torque control with SVM for sensorless induction motor using sliding mode controller and observer. *Int. J. Computer Aided Engineering and Technology*, Vol. 11, No. 1, pp.14-34.

[25] El Azzaoui, M., Mahmoudi, H., Ed-dahmani, C. (2016). Backstepping Control of a Doubly Fed Induction Generator Integrated to Wind Power System. *2nd International Conference on Electrical and Information Technologies, ICEIT'2016*.

[26] Chen, C., Yu., H, Gong, F., Wu., H. (2020). Induction Motor Adaptive Backstepping Control and Efficiency Optimization Based on Load Observer. *Energies*, 13, 3712

[27] Ali, S., Prado, A., Pervaiz, M. (2023). Hybrid Backstepping-Super Twisting Algorithm for Robust Speed Control of a Three-Phase Induction Motor. *Electronics*, 12, 681.

Contribution of Individual Authors to the Creation of a Scientific Article (Ghostwriting Policy)

The authors equally contributed in the present research, at all stages from the formulation of the problem to the final findings and solution.

Sources of Funding for Research Presented in a Scientific Article or Scientific Article Itself

No funding was received for conducting this study.

Conflict of Interest

The authors have no conflicts of interest to declare.